

# Search for WIMP Inelastic Scattering Off Xenon Nuclei With Xenon100 Data

M. Alfonsi,<sup>1</sup> E. Aprile,<sup>2</sup> K. Arisaka,<sup>3</sup> F. Arneodo,<sup>4</sup> C. Balan,<sup>5</sup> L. Baudis,<sup>6</sup> A. Behrens,<sup>6</sup> P. Beltrame,<sup>3</sup> K. Bokeloh,<sup>7</sup> E. Brown,<sup>7</sup> G. Bruno,<sup>4</sup> R. Budnik,<sup>2</sup> J. M. R. Cardoso,<sup>5</sup> W.-T. Chen,<sup>8</sup> B. Choi,<sup>2</sup> H. Contreras,<sup>2</sup> J. P. Cussonneau,<sup>8</sup> M. P. Decowski,<sup>1</sup> E. Duchovni,<sup>9</sup> S. Fattori,<sup>10</sup> A. D. Ferella,<sup>6</sup> W. Fulgione,<sup>11</sup> F. Gao,<sup>12</sup> M. Garbini,<sup>13</sup> K.-L. Giboni,<sup>2</sup> L. W. Goetzke,<sup>2</sup> C. Grignon,<sup>10</sup> E. Gross,<sup>9</sup> W. Hampel,<sup>14</sup> H. Kettling,<sup>7</sup> A. Kish,<sup>6</sup> J. Lamblin,<sup>8</sup> H. Landsman,<sup>9</sup> R. F. Lang,<sup>15,2</sup> M. Le Calloch,<sup>8</sup> C. Levy,<sup>7</sup> K. E. Lim,<sup>2</sup> Q. Lin,<sup>12</sup> S. Lindemann,<sup>14</sup> M. Lindner,<sup>14</sup> J. A. M. Lopes,<sup>5</sup> K. Lung,<sup>3</sup> T. Marrodán Undagoitia,<sup>6,\*</sup> F. V. Massoli,<sup>13</sup> Y. Mei,<sup>16,10</sup> A. J. Melgarejo Fernandez,<sup>2</sup> Y. Meng,<sup>3</sup> A. Molinario,<sup>11</sup> E. Nativ,<sup>9</sup> K. Ni,<sup>12</sup> U. Oberlack,<sup>16,10</sup> S. E. A. Orrigo,<sup>5</sup> E. Pantic,<sup>3,†</sup> D. Pätzold,<sup>10</sup> R. Persiani,<sup>13</sup> G. Plante,<sup>2</sup> N. Priel,<sup>9</sup> A. C. C. Ribeiro,<sup>5</sup> A. Rizzo,<sup>2</sup> S. Rosendahl,<sup>7</sup> J. M. F. dos Santos,<sup>5</sup> G. Sartorelli,<sup>13</sup> J. Schreiner,<sup>14</sup> M. Schumann,<sup>6</sup> L. Scotto Lavina,<sup>8</sup> P. R. Scovell,<sup>3</sup> M. Selvi,<sup>13</sup> P. Shagin,<sup>16</sup> H. Simgen,<sup>14</sup> A. Teymourian,<sup>3</sup> D. Thers,<sup>8</sup> O. Vitells,<sup>9</sup> H. Wang,<sup>3</sup> M. Weber,<sup>14</sup> and C. Weinheimer<sup>7</sup>

(The XENON100 Collaboration)

<sup>1</sup>*Nikhef and the University of Amsterdam, Science park, Amsterdam, Netherlands*

<sup>2</sup>*Physics Department, Columbia University, New York, NY 10027, USA*

<sup>3</sup>*Physics & Astronomy Department, University of California, Los Angeles, USA*

<sup>4</sup>*INFN, Laboratori Nazionali del Gran Sasso, Assergi, 67100, Italy*

<sup>5</sup>*Department of Physics, University of Coimbra, R. Larga, 3004-516, Coimbra, Portugal*

<sup>6</sup>*Physics Institute, University of Zürich, Winterthurerstr. 190, CH-8057, Switzerland*

<sup>7</sup>*Institut für Kernphysik, Wilhelms-Universität Münster, 48149 Münster, Germany*

<sup>8</sup>*SUBATECH, Ecole des Mines de Nantes, CNRS/In2p3, Université de Nantes, 44307 Nantes, France*

<sup>9</sup>*Department of Particle Physics and Astrophysics, Weizmann Institute of Science, 76100 Rehovot, Israel*

<sup>10</sup>*Institut für Physik, Johannes Gutenberg Universität Mainz, 55099 Mainz, Germany*

<sup>11</sup>*University of Torino and INFN-Torino, Torino, Italy*

<sup>12</sup>*Department of Physics, Shanghai Jiao Tong University, Shanghai, 200240, China*

<sup>13</sup>*University of Bologna and INFN-Bologna, Bologna, Italy*

<sup>14</sup>*Max-Planck-Institut für Kernphysik, Saupfercheckweg 1, 69117 Heidelberg, Germany*

<sup>15</sup>*Department of Physics, Purdue University, West Lafayette, IN 47907, USA*

<sup>16</sup>*Department of Physics and Astronomy, Rice University, Houston, TX 77005 - 1892, USA*

(Dated: January 9, 2017)

Some nice abstract here.....

## I. INTRODUCTION

Astrophysical evidence indicates that the dominant mass fraction of our Universe consists of some yet unknown form of dark matter. Well motivated models predict Dark Matter in the form of Weakly Interacting Massive Particles (WIMPs), hypothesis which is currently being tested by several direct and indirect detection experiments. [some citation missing](#).

Most of direct detection searches focuses on elastic scattering of dark matter particles off nuclei. In this analysis instead an inelastic scattering process is explored, we consider the  $^{129}\text{Xe}$  isotope being excited to a low-lying state with subsequent prompt de-excitation via the emission a photon. This isotope is an excellent target since its abundance in natural xenon is of 26.4% and a relatively low energy is necessary to excite its  $3/2^+$  state above the  $1/2^+$  spin ground state. These type of processes were previously studied in detail for liquid xenon detector in [1]. Inelastic WIMP-nucleus scattering in xenon is complementary to elastic scattering for spin-dependent

interactions, the former dominates the integrated rate above  $\simeq 10$  keV of energy deposition. Furthermore, in the case of dark matter detection, this channel can be employed to asses whether the nature of the fundamental interaction is spin-dependent or not.

## II. XENON100 DETECTOR

The Xenon100 experiment is a dual phase liquid xenon TPC. For a given interaction in the liquid target this type of detector produces two separated signals, one proportional to the prompt scintillation (S1) the other to ionization (S2).

To add: describe and explain cS1 and cS2 definitions, [some sentences about detector stability](#), [maybe science run data used and calibration campaign goes here](#), [maybe Ly and Y measurements used goes here](#).

## III. DATA ANALYSIS

This analysis is performed using XENON100 Run-II science data, which corresponds to an exposure of 224.6 live days. The detector response to electronic re-

\* marrodan@physik.uzh.ch

† pantic@physics.ucla.edu

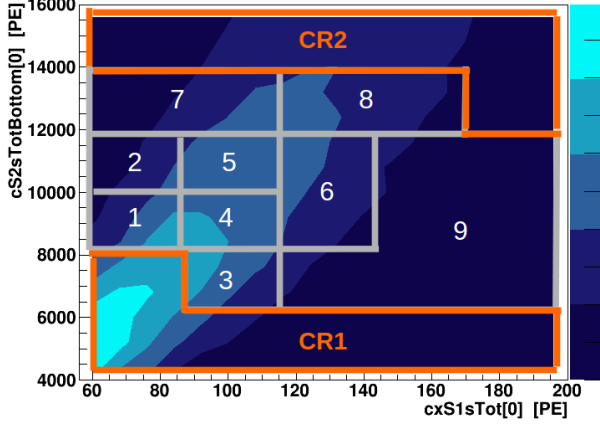


FIG. 1. Signal region and control region.

coil (ER) has been characterized using  $^{60}\text{Co}$  and  $^{232}\text{Th}$  radioactive sources, while response to inelastic nuclear recoil (NR) scattering was calibrated using an  $^{241}\text{AmBe}$  source.

The inelastic scattering of a WIMP with the nucleus of  $^{129}\text{Xe}$  produces an energy deposit via nuclear recoil with subsequent emission of a 39.6 KeV de-excitation photon. The largest fraction of the energy released in the event is via electronic recoil due to the emitted photon, this represents an unusual signature for this kind of detector and brings the possible signal to overlay a phase space region with large backgrounds. The chosen region of interest for this analysis surrounds the 39.6 KeV xenon line in the cS1-cS2 plane which is further divided into sub-regions, as shown in Figure 1.

Events are asked, other than falling in the defined region of interest, to fulfill several selection criteria which can be summarized as: selection aimed to reduce noise impact including energy (S1) and S2 thresholds, events must be of single scatter nature and fall into a predefined fiducial volume. This analysis follows the selection criteria described in detail in [2] for Run-II, with only few exceptions. In particular, the selection on S2 width as a function of drift time has been optimized on a sample of events selected from the 39.6 KeV line and set to a 95% acceptance on these. Events are required to be single scatter by applying a threshold on the second largest S2 peak size, for this analysis this threshold has been optimized to 160 PE and set constant as function of S2 signal size. Finally the chosen fiducial volume corresponds to 34 Kg of liquid xenon.

### A. Signal Simulation

The detector response to inelastic scattering of WIMPs off  $^{129}\text{Xe}$  nucleus was simulated using an empirical model. The total deposited energy is divided into two independent contributions: the one related to the 39.6 KeV de-

excitation photon and the one relative to the simultaneous nuclear recoil of the xenon atom, the number of photons and charge yield detected is simulated separately for each contribution and then added together.

The ER induced by the de-excitation photon is simulated assuming a two dimensional normal distribution as its pdf in the cS1-cS2 plane,  $f(cS1, cS2)$ , described (except a normalization factor) in equation 1:

$$f(cS1, cS2) = \exp\left(-\frac{1}{2(1-\rho^2)}\left[\frac{(cS1 - \mu_{cS1})^2}{\sigma_{cS1}^2} + \frac{(cS2 - \mu_{cS2})^2}{\sigma_{cS2}^2} - \frac{2\rho(cS1 - \mu_{cS1})(cS2 - \mu_{cS2})}{\sigma_{cS1}\sigma_{cS2}}\right]\right) \quad (1)$$

where  $\mu_{cS1}$  and  $\mu_{cS2}$  represents the average observed cS1 and cS2 given a 39.6 KeV ER,  $\sigma_{cS1}$  and  $\sigma_{cS2}$  are the standard deviation in cS1 and cS2 respectively, while  $\rho$  stands for the correlation between cS1 and cS2. The detector related light yield  $L_y$  measured at 39.6 KeV, necessary to evaluate the average number of photon detected ( $\mu_{cS1}$ ), is obtained as the result of a NEST model [3–5] fit to data collected with several lines. The same model is used to predict the charge yield at 39.6 KeV which is then scaled according to the detector's secondary scintillation gain  $Y$ , determined from detector response to single electrons [6]. Note that the corrected S2 observed by the bottom PMT array is used in this analysis. The detector resolution at 39.6 KeV in cS1 and cS2 has been measured to be respectively 15.8% and 14.7% and used to extract the standard deviations  $\sigma_{cS1}$ ,  $\sigma_{cS2}$ . The correlation parameter is assumed to be independent of energy (at least in the considered range) and measured using the 164 KeV xenon activated line by  $^{124}\text{AmBe}$  calibration data, this line is chosen since allows to disentangle efficiently contribution from nuclear recoil. The measured correlation is  $\rho = -0.45 \pm 0.10$ .

The cS1 and cS2 distributions from NR contribution are predicted starting from the nuclear recoil energy spectrum for WIMPs inelastic interaction [1]. The average cS1 and cS2 are given by equations 2 and 3 respectively, where  $\mathcal{L}_{eff}$  is the liquid xenon NR relative scintillation efficiency while  $S_{ee} = 0.58$  and  $S_{nr} = 0.95$  describe the scintillation quenching due to the electric field [7]. The parameterization and uncertainties of  $\mathcal{L}_{eff}$  as a function of  $E_{nr}$  are based on existing direct measurements [8]. The light yield at 122 keVee originate from the same NEST model fit as described above. For the cS2 the parameterization of  $Q_Y(E_{nr})$  is taken from [9]. Finally all detector related resolution effects are introduced following the prescriptions described in [2].

$$cS1_{nr} = E_{nr} \mathcal{L}_{eff}(E_{nr}) L_y \frac{S_{nr}}{S_{ee}} \quad (2)$$

$$cS2_{nr} = E_{nr} Q_Y(E_{nr}) Y \quad (3)$$

The pdf of the ER and NR contributions are then convoluted together to obtain the overall pdf of the signal.

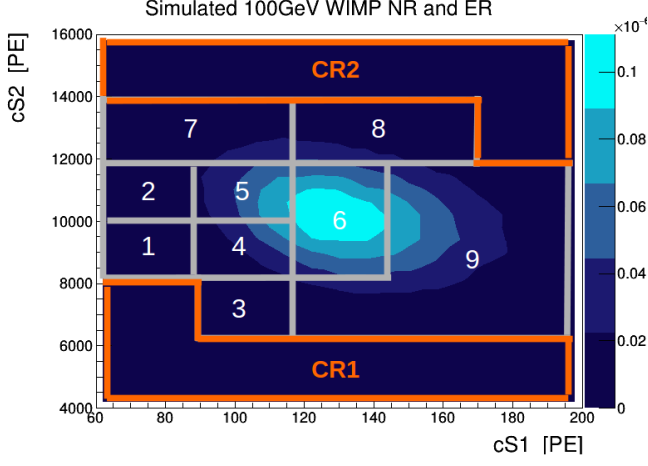


FIG. 2. Signal region and control region, for WIMP of mass 100 GeV.

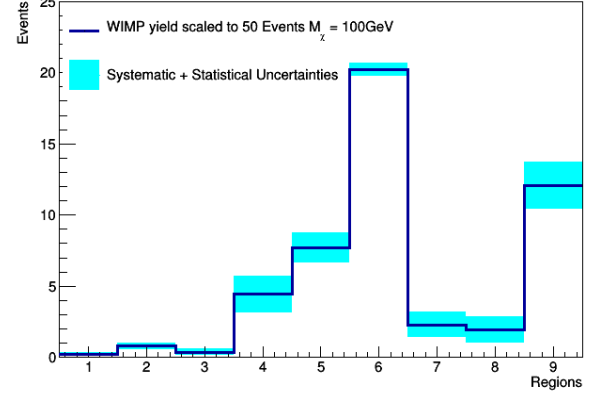


FIG. 3. Signal region, uncertainties for WIMP of mass 100 GeV.

A 2D (cS1 versus cS2) acceptance map is applied to the signal pdf to reproduce data selection effects. Acceptances are computed separately for each selection criteria using  $^{124}\text{AmBe}$  calibration sample, selections as the outer volume veto and the single scatter interaction represent an exception and a detailed computation has been performed in these cases. The acceptance average in the region of interest to about  $0.80 \pm 0.05$ . Figure 1 shows an example of full simulated signal model for a WIMP of 100 GeV mass.

The signal simulation procedure has been validated reproducing the 39.6 KeV xenon line from interaction due to  $^{124}\text{AmBe}$  source and has been compared to data. For the comparison the proper  $^{124}\text{AmBe}$  nuclear recoil and acceptances were simulated. The simulated events were found in agreement with calibration data within statistical uncertainties.

## B. Background Model

The main expected background contribution in the region of interest is due material radioactivity, composed mainly by photons interacting via compton scattering. Background contribution due to the activation of the xenon 39.6 KeV line from radiogenic neutrons is expected to be negligible. The background is modeled using data from  $^{60}\text{Co}$  calibration campaign, which are assumed to well represent the background density distribution in the cS1-cS2 plane.

The calibration sample yields about 22'000 events in the ROI, these are then scaled to data according to a measured background scale factor  $\tau_{bkg}$ . The scale factor is measured in the two control regions shown in Figure 1 and labelled CR1 and CR2. The two control regions give compatible results and the computed average is  $\tau_{bkg} = 0.034 \pm 0.002$ , where the reported uncertainty is of statistical nature only.

The distribution of the calibration sample has been compared to the data of the science run in the two control regions, agreement is found within statistical uncertainties.  $^{60}\text{Co}$  calibration data have been compared in the region of interest to data from  $^{232}\text{Th}$  calibration campaign, the largest deviation between the two shapes is within 4%. An additional systematic uncertainty of 4% has been applied to the expected background yield of each sub-region of the ROI.

## C. Systematic Uncertainties

Uncertainties on the total prediction of background events arise from the uncertainty on the measure of the normalization factor,  $\tau_{bkg}$ , and amount to 6%, contribution of radiogenic neutrons are neglected. Systematic uncertainty on the shape of the predicted background distribution are assessed by the maximal discrepancy in the ROI between the  $^{60}\text{Co}$  and  $^{232}\text{Th}$  calibration samples, a 4% systematic additional to statistical uncertainty is assigned to the expected yield of each sub-region, note that uncertainties belonging to different sub-regions are considered independent from each other.

Signal model, Energy scale uncertainties.... Uncertainties related to energy scale and more generally to detector response are taken into account by relative uncertainties on the measure of  $L_y, \mathcal{L}_{eff}, Y, Q_Y$  and  $\rho$ . Has been shown by the simulation that these type of uncertainty affect the total signal yield in the ROI by less than a percent for a wide range of masses, however they greatly affects the pdf of the signal model in the ROI. For each WIMP mass several signal simulation sample are produced varying these parameter respectively  $\pm 1\sigma$ , for each region is computed an uncertainty by adding in quadrature the variations with respect to nominal of each case, Figure 3 is an example of such a systematic uncertainty computation for WIMP mass of 100 GeV.

Uncertainty on the total yield of the signal arising from

uncertainties on the selection acceptance are found to be very weakly dependent on the WIMP mass, an overall 6% acceptance uncertainty is then applied to all WIMP hypothesis.

All the uncertainties discussed here are threatened as nuisance parameter in the likelihood, which are constrained by a gaussian distribution.

#### IV. RESULTS

In an exposure of 34 Kg per 224 days of liquid xenon a yield of 764 events are found in the region of interest, which is compatible with the expectation of  $756 \pm 5^{(stat.)} \pm 55^{(syst.)}$ . The distribution of events from data are compared to the background expectation in Figure 4 and with the relative uncertainties. This result is interpreted via a binned profiled likelihood approach by means of the test statistic  $\tilde{q}$  and its asymptotic distributions described in [10]. 90% CL<sub>s</sub> [11] confidence level limits are computed on the spin dependent cross section as a function of the WIMP mass and shown in Figure 5.

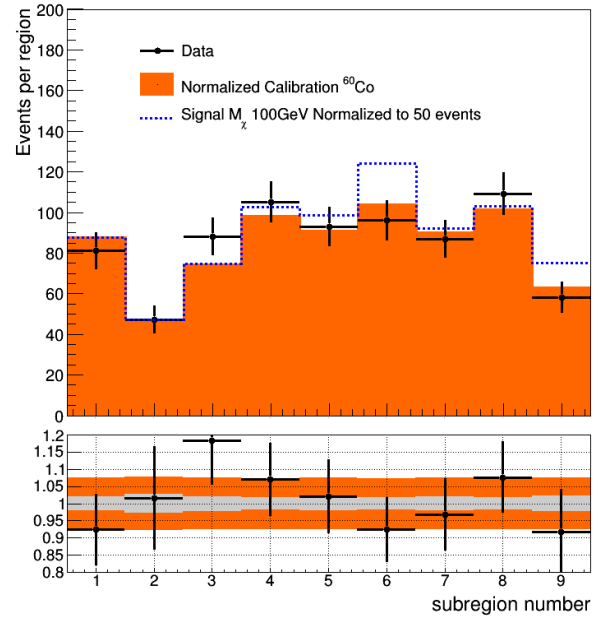


FIG. 4. Results, comparison between data and expected background.

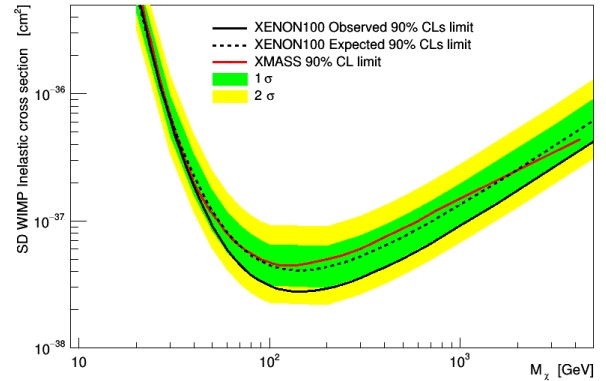


FIG. 5. Observed and expected limits.

- 
- [1] L. Baudis, G. Kessler, P. Klos, R. F. Lang, J. Men-  
 ndez, S. Reichard, and A. Schwenk. Signatures of Dark  
 Matter Scattering Inelastically Off Nuclei. *Phys. Rev.*,  
 D88(11):115014, 2013.
- [2] E. Aprile et al. XENON100 Dark Matter Results  
 from a Combination of 477 Live Days. *Phys. Rev.*,  
 D94(12):122001, 2016.
- [3] M Szydagis, A Fyhrie, D Thorngren, and M Tripathi. En-  
 hancement of nest capabilities for simulating low-energy  
 recoils in liquid xenon. *Journal of Instrumentation*,  
 8(10):C10003, 2013.
- [4] John Allison et al. Geant4 developments and applica-  
 tions. *IEEE Trans. Nucl. Sci.*, 53:270, 2006.
- [5] S. Agostinelli et al. GEANT4: A Simulation toolkit.  
*Nucl. Instrum. Meth.*, A506:250–303, 2003.
- [6] E Aprile et al. Observation and applications of single-  
 electron charge signals in the xenon100 experiment.  
*Journal of Physics G: Nuclear and Particle Physics*,  
 41(3):035201, 2014.
- [7] E. Aprile, C. E. Dahl, L. DeViveiros, R. Gaitskell, K. L.  
 Giboni, J. Kwong, P. Majewski, Kaixuan Ni, T. Shutt,  
 and M. Yamashita. Simultaneous measurement of ioniza-  
 tion and scintillation from nuclear recoils in liquid xenon  
 as target for a dark matter experiment. *Phys. Rev. Lett.*,  
 97:081302, 2006.
- [8] E. Aprile et al. Dark Matter Results from 100 Live Days  
 of XENON100 Data. *Phys. Rev. Lett.*, 107:131302, 2011.
- [9] E. Aprile et al. Response of the XENON100 Dark Matter  
 Detector to Nuclear Recoils. *Phys. Rev.*, D88:012006,  
 2013.
- [10] Glen Cowan, Kyle Cranmer, Eilam Gross, and Ofer  
 Vitells. Asymptotic formulae for likelihood-based tests  
 of new physics. *Eur. Phys. J.*, C71:1554, 2011. [Erra-  
 tum: *Eur. Phys. J.* C73,2501(2013)].
- [11] Alexander L. Read. Modified frequentist analysis of  
 search results (The CL(s) method). In *Workshop on con-  
 fidence limits, CERN, Geneva, Switzerland, 17-18 Jan  
 2000: Proceedings*, pages 81–101, 2000.